Pressure induced Lifshitz transition in ThFeAsN

Smritijit Sen[1] and Guang-Yu Guo[1,2,*]

[1]*Department of Physics and Center for Theoretical Physics, National Taiwan University, Taipei 10617, Taiwan*

[2]*Physics Division, National Center for Theoretical Sciences, Hsinchu 30013, Taiwan*

(Received 20 April 2020; accepted 7 October 2020; published 27 October 2020)

In this paper, we present pressure dependent structural parameters and electronic structure of the ThFeAsN superconductor. There are no anomalies in the structural parameters as well as elastic constants with hydrostatic pressure which is consistent with the experiments. We study the electronic structure of this compound at different external pressures in terms of density of states, band structure, and Fermi surface. Density of states at the Fermi level, coming from Fe-d orbitals, follows the same trend as that of the superconducting transition temperature (T_c) as a function of hydrostatic pressure. We also observe a pressure induced orbital selective Lifshitz transition in ThFeAsN compound which is quite different from the Lifshitz transitions observed in the other families of Fe-based superconductors. Fermi surfaces of ThFeAsN especially holelike Fermi surfaces at the Γ point are altered significantly with pressure. This modification of Fermi surface topology with pressure seems to play a major role in the reduction of T_c with pressure in ThFeAsN superconductor. Spin-orbit coupling does not affect the Lifshitz transition but it modifies the energy ordering of bands near the Γ point at higher pressure.

DOI: 10.1103/PhysRevMaterials.4.104802

I. INTRODUCTION

Fe-based superconductors display a number of exotic normal state characteristics apart from its quirky superconducting properties [1]. Proximity of magnetism and superconductivity make these systems even more interesting and versatile [2–4]. The presence of superconducting order along with the structural phase transition, spin density wave (SDW) order, orbital density wave order (ODW), nematic order, Lifshitz transition/electronic topological transition etc., construct a very complex phase diagram for Fe-based superconductors [5–13]. These phases are also very sensitive to external parameters like temperature, pressure, doping etc. [14–18]. It is a well established fact that pressure is an important controlling parameter of superconducting transition temperature (T_c) for high temperature superconductors in general and Fe-based superconductors are no exception to that [19–22]. For example, $BaFe_2As_2$ (belongs to the 122 family) is a parent compound of Fe-based superconductor that possesses a SDW ground state with no superconducting properties, but hydrostatic pressure or chemical pressure (doping in any of the three sites) can induce superconductivity with a T_c as high as 30 K [23–25]. One more example is FeSe (belongs to the 11 family), which is a superconductor with a T_c of 8.5 K. However, this T_c can be lifted up to 36.7 K with the application of hydrostatic pressure of 9 GPa [26]. In addition to that, pressure can be regarded as a reliable parameter for investigating the influence of structural disorder on electronic structures. In Fe-based superconductors, electronic structure and structural parameters like 'anion height' (distance of the As/Se atom from the Fe plane) and tetrahedral bond angle α (As-Fe-As) are closely connected and tune the superconducting T_c [27,28]. Moreover, recent studies reveal that spin-orbit coupling (SOC) plays a crucial role in Fe-based superconductors [29] as it lifts the degeneracy of Fe-d_{xz} and Fe-d_{yz} orbitals at the Γ point which results in an orbital ordering in the FeTe(Se) system [30,31].

Lifshitz transition is an electronic topological transition of the Fermi surface where symmetry is preserved [32]. At $T = 0$ K, Lifshitz transition is a true phase transition of order $2\frac{1}{2}$ (Ehrenfest's classification). Lifshitz transition (LT)/electronic topological transition (ETT) is an integral part of Fe-based superconductivity and is found to play a significant role in tuning the superconducting transition temperature owing to its multiorbital nature of Fermi surface (FS). LT is observed in Fe-based superconductors induced by hydrostatic pressure, external magnetic field, impurity, and doping [33–37]. In particular, pressure induced LT transition is observed on the verge of tetragonal to collapse tetragonal transition in 122 pnictides [19]. A number of experimental as well as theoretical studies reveal the occurrence of LT in the $BaFe_2As_2$ system with doping which influences the superconducting properties enormously [38–40]. One of the important outcomes of these studies is that LT occurs in the holelike FSs for electron doping and vice versa. The consequences of LT/ETT are innumerable. Lifshitz transition moderates the low energy electronic structure, such as creation or disappearance of a Fermi pocket or formation of Fermi surface neck or bottle, developing typical topological modifications. In general, LT is interlinked with the crossing of van Hove singularity at the Fermi level. However, this may not be that simple to intuit in a complex multiorbital system like Fe-based superconductor. At finite temperature, LT can be identified by the anomalies in the behavior of lattice parameters, density of states near the Fermi level, elastic properties and electron dynamics as manifested in the experimental observable like thermal and

*Corresponding author: gyguo@phys.ntu.edu.tw

transport properties [32,41]. In recent days, angle resolved photoemission spectroscopy (ARPES) experiments are more than capable of mapping FS topology with temperature, pressure, and doping [42,43]. Therefore, it can be used to detect LT/ETT experimentally.

Recently, a new member of the 1111 Fe-based family, ThFeAsN, has been synthesized with a reported T_c of 30 K in the stoichiometric compound in ambient pressure [44]. ThFeAsN is distinctively different from its fellow members of the 1111 Fe-based family in spite of possessing the same crystal structure. For example, ThFeAsN is an intrinsic superconductor without doping and external pressure. On the other hand, superconductivity arises in LaOFeAs only if we dope F in O sites. No long range magnetic order has been observed in ThFeAsN on the contrary to an antiferromagnetic ground state in the LaOFeAs system. Although, strong magnetic fluctuations above 35 K have been reported [45]. Moreover, ThFeAsN has no structural phase transition in contrast to the structural phase transition from high temperature tetragonal phase to low temperature orthorhombic phase in LaOFeAs, although a weak structural disorder at around 160 K is observed in ThFeAsN [46]. Our recent study reveals that the phonon does not play a significant role in the superconductivity of ThFeAsN [47]. The effect of pressure in the superconducting properties of ThFeAsN has also been studied experimentally [48,49]. Wang *et al.* show that the superconducting transition temperature gradually decreases with the increase of external pressure and eventually superconductivity disappears at about 25.4 GPa of hydrostatic pressure. This work also established that the universal trends of superconducting T_c and anion height/α are followed by the ThFeAsN system [28,48]. However electronic structure at high pressure and its implications on superconductivity are still missing in the current literature.

In this work, we provide a detailed systematic evolution of electronic structures as well as structural parameters with external pressure up to 35 GPa. We also show the modifications of FS topology and electronic band structure induced by pressure, leading to an orbital selective LT. We also study the influence of SOC in the electronic structure of ThFeAsN at higher pressure.

II. CRYSTAL STRUCTURE AND COMPUTATIONAL METHODS

The crystal structure of ThFeAsN is tetragonal with space group symmetry $P4/nmm$ (space group no. 129). The schematic diagram of tetragonal ThFeAsN crystal is presented in Fig. 1. The unit cell consists of two formula units (f.u.). Experimental lattice parameters of tetragonal ThFeAsN ($a = 4.0305$ Å, $c = 8.5169$ Å) are used as the input of our first principles density functional theory calculations [48]. Experimentally no long range magnetic order has been observed in the ThFeAsN system. Therefore, magnetism is not considered in our first principles calculations. Our first principles calculations were performed by employing the projector augmented-wave (PAW) method as implemented in the Vienna *ab initio* simulation package (VASP) [50–52]. The exchange correlation functional has been treated under generalized-gradient approximation (GGA) within the Perdew-Burke-Ernzerhof (PBE) functional [53]. Electron correlation can be an important factor in Fe based materials. However, most of the Fe based superconductors except FeSe systems, show weak or moderate correlation strength [54]. In order to see the role of electron correlation in ThFeAsN in ambient pressure, we further study the effect of electron correlation on the electronic structure especially DOS, by performing the so-called GGA+U calculations [55] where a moderate value of effective onsite Coulomb repulsion U is included and the results are presented in Appendix A.

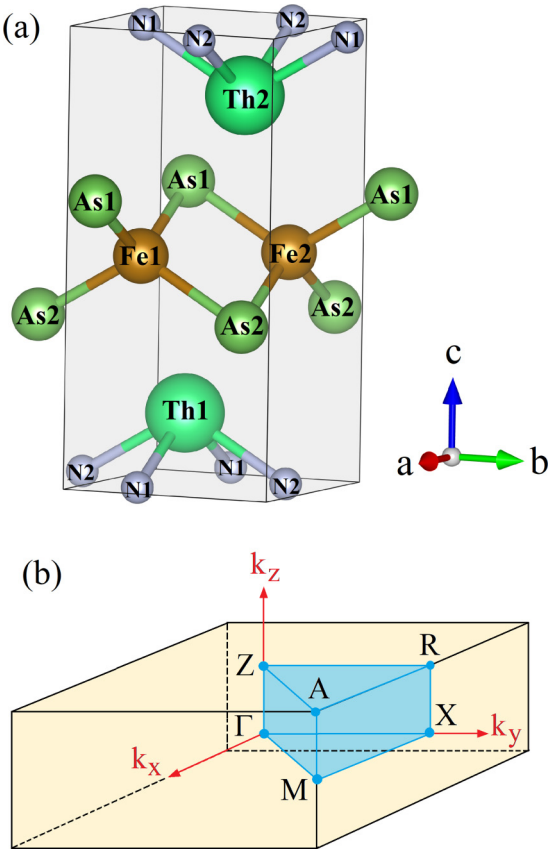

FIG. 1. (a) Crystal structure and (b) Brillouin zone of tetragonal ThFeAsN.

All the lattice parameters as well as internal atomic positions are relaxed with an energy convergence of 10^{-8} eV. The wave functions were expanded in the plane waves basis with an energy cutoff of 600 eV. The sampling of the Brillouin zone was done using a Γ-centered $10 \times 10 \times 5$ Monkhorst-Pack grid. To obtain the crystal structures at different pressures, we begin with the $P = 0$ structure. Then, we optimize the lattice parameters and atomic positions in the presence of hydrostatic pressure (up to 35 GPa). Electronic structure calculation is performed using these optimized crystal structures at a particular external pressure. Elastic constants were calculated within VASP by finite differences of stress with respect to strain [56]. The forces and stresses of the final converged structures were optimized and checked to be within the error allowance of the VASP code. For the Fermi surface calculations, a denser k grid of size $20 \times 20 \times 20$ is considered.

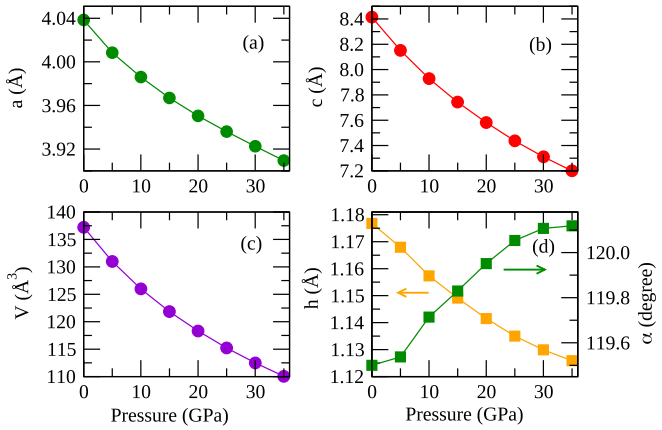

FIG. 2. Pressure dependencies of lattice parameters (a) a, (b) c, (c) volume of unit cell, (d) anion height (distance of As atom from Fe plane) and As-Fe-As bond angle α.

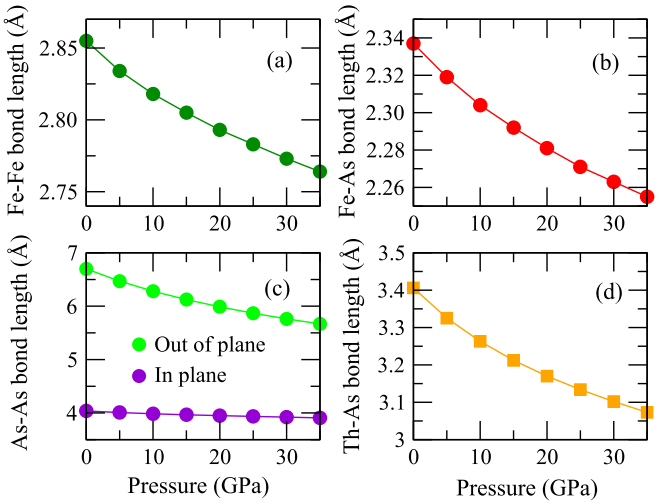

FIG. 3. (a) Fe-Fe bond length, (b) Fe-As bond length, (c) in-plane and out of plane As-As bond length, (d) Th-As bond length of ThFeAsN as a function of hydrostatic pressure.

III. RESULTS AND DISCUSSION

A. Evolution of crystal structure with pressure

We start with the calculated pressure dependent structural parameters. In Fig. 2, we present our calculated lattice parameters, volume of unit cell, anion height, and bond angle (α) as a function of hydrostatic pressure. For tetragonal ThFeAsN compound, lattice parameters a and c both gradually decrease with the increasing pressure. As a result of this, unit cell volume also decreases with the increasing pressure [see Fig. 2(c)]. Anion height is also reduced as we move in the higher values of hydrostatic pressure. Not only volume but c/a ratio also monotonically decreases with the increasing external pressure. On the other hand, As-Fe-As bond angle increases with the pressure. Structural parameters like anion height and As-Fe-As bond angle play an important role in superconductivity of Fe-based superconductors [28,57]. Our calculated pressure dependencies of these structural parameters are consistent with the experiments [48]. Variations of anion height and As-Fe-As bond angle with external pressure follow the experimental trends only qualitatively. The experimental value of anion height at ambient pressure is 1.31 Å and our calculated anion height at ambient pressure is 1.17 Å. Optimized value of anion height within density functional theory (using GGA-PBE exchange-correlation functional) at ambient pressure is much lower than the experimentally measured value of anion height. This well addressed discrepancy of anion height calculation of Fe-based superconductors using *ab initio* density functional theory is due to the magnetic fluctuation associated with the Fe atoms, present in the Fe-based superconductors [58–60]. Our current system has no long range magnetic order but tends to show strong magnetic fluctuation above 35 K [45]. Therefore, the underestimation of anion height is consistent with the current literature [18,60]. However, at higher pressure our calculated anion heights as well as As-Fe-As bond angles resemble that of the experimental values. This also may give an indication of reduction of magnetic fluctuation in the system at higher pressure. Incidentally, superconducting transition temperature also decreases abruptly at higher pressure indicating that magnetic fluctuation may have influence over the superconducting properties in ThFeAsN. Therefore, it demands further investigation to find if there is any connection between magnetic fluctuation and superconductivity in this material. At low temperature, van der Waals interaction can be a contributing factor for layered materials such as ThFeAsN. However, recent studies by other researchers reveal that for the FeSe system (belongs to the 11 family of Fe based superconductors) van der Waals interaction plays a significant role in determining the crystal structure while the crystal structure of other families of Fe based superconductors are not so sensitive to van der Waals interaction [61,62]. We have also performed structural optimizations for ThFeAsN at ambient pressure including van der Waals correction. The van der Waals interaction is considered using the zero damping DFT-D3 method of Grimme [63] as implemented in VASP code. Our calculated value of anion height including van der Waals correction is 1.18 Å. From our calculation it is quite clear that van der Waals interaction does not play a significant role in ThFeAsN. We also show the behavior of various bond lengths as a function of pressure. In Fig. 3, we depict the variation of Fe-Fe, Fe-As, As-As (in plane and out of plane), and Th-As bond lengths with pressure. All the bond lengths shrink as we move towards higher pressure. Smooth behavior of the structural parameters as a function of hydrostatic pressure suggests that there is no structural transition in ThFeAsN at higher pressure up to 35 GPa. Experimentally also, no structural phase transition is observed in ThFeAsN compound at higher pressure (up to 29.4 GPa of hydrostatic pressure). Variation of out of plane As-As distance is more prominent than that of the in plane one. This indicates that there is a possibility of significant modifications in the electronic structure along the z axis as compared to that in the xy plane. We also calculate the elastic constants of the tetragonal ThFeAsN system at various hydrostatic pressures.

In Fig. 4, we depict our calculated elastic constants of ThFeAsN as a function of pressure. There are six elastic constants in the tetragonal ThFeAsN system. All six elastic

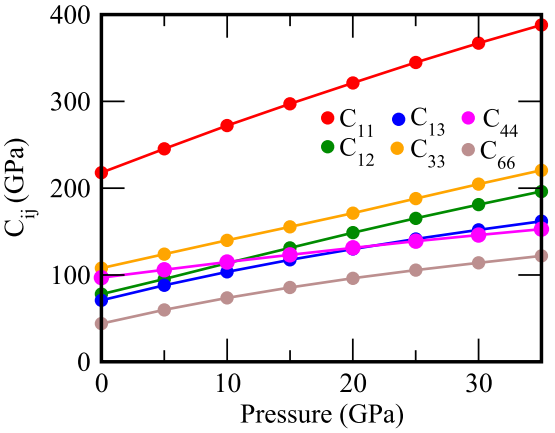

FIG. 4. Pressure variation of elastic constants of tetragonal ThFeAsN.

constants (C_{11}, C_{12}, C_{13}, C_{33}, C_{44}, C_{66}) increase monotonically with pressure. All the elastic constants are positive and obey the well known Born criterion of mechanical stability [64] throughout the pressure range that we considered. The absence of anomalies in the pressure variation of elastic constants indicates that there is no structural disorder (like collapse tetragonal phase as observed in some of the other Fe-based superconductors [19]). In the next section, we present our calculated electronic structure at various external pressures.

B. Electronic structure and Lifshitz transition

Our electronic structure calculation at different hydrostatic pressures consists of density of states (DOS), electronic band dispersions, and Fermi surfaces (FSs). First, we display our calculated total density of states at different hydrostatic pressures. In Fig. 5, we present our calculated total density of states for 4, 10, 15, 20, and 25 GPa of hydrostatic pressure along with the ambient one. There are some visible changes in the DOS as a function of hydrostatic pressure. Since Fe-*d* orbitals and As-*p* orbitals mainly constitute the low energy electronic structure of most of the Fe-based superconductors, we study the Fe-*d* and As-*p* orbital-projected DOS at different

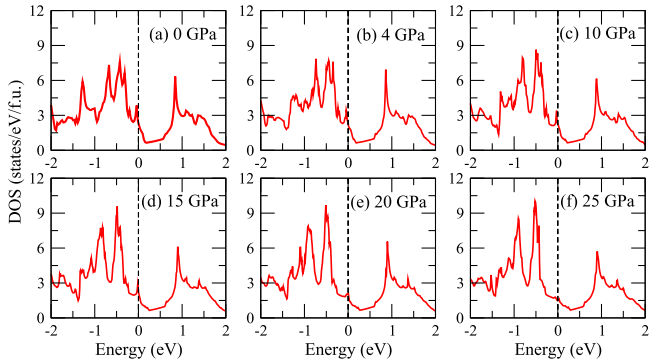

FIG. 5. Calculated total density of states of tetragonal ThFeAsN at (a) ambient, (b) 4 GPa, (c) 10 GPa, (d) 15 GPa, (e) 20 GPa, and (f) 25 GPa pressure. Fermi level is denoted by a vertical line at $E = 0$ eV.

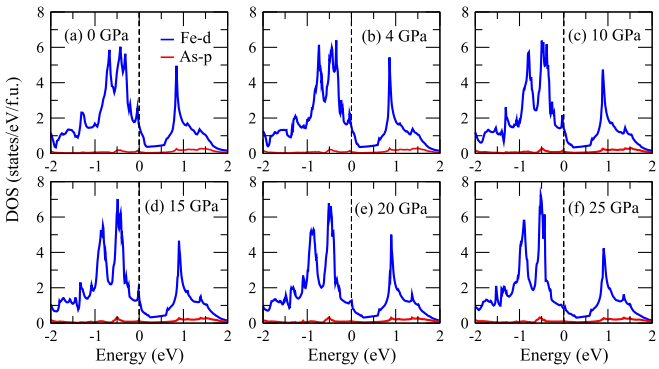

FIG. 6. Calculated atom projected density of states of tetragonal ThFeAsN at (a) ambient, (b) 4 GPa, (c) 10 GPa, (d) 15 GPa, (e) 20 GPa, and (f) 25 GPa pressure.

pressures. In Fig. 6, we display our calculated Fe-*d* and As-*p* orbital-projected DOS at ambient and 4, 10, 15, 20, 25 GPa of hydrostatic pressure. We observe that As-*p* orbital has very little contribution in the low energy electronic density of states at all pressure ranging from 0 to 35 GPa as compared to the contributions from the Fe-*d* orbitals. We also calculate the DOS at Fermi level for Fe-*d* states N_{E_F}(Fe) at each pressure and in Fig. 7, we show the pressure dependencies of N_{E_F}(Fe). In the same plot, we also depict the variation of experimentally measured superconducting T_c of ThFeAsN with pressure [48]. It is quite evident from Fig. 7 that the variation of Fe-*d* DOS at the Fermi level with pressure follows the same trend as that of the superconducting T_c measured experimentally [48] at different pressures. DOS at the Fermi level drops significantly with pressure and a sharp fall around 20 GPa of pressure is observed. This in turn reduces the possibility of electron pairing at higher pressure. We speculate this may be one of the reasons that superconducting T_c decreases with the increasing pressure. We also calculate the variation of Fe-*d* orbital resolved DOS with pressure. In Figs. 8(a)–8(d), 8(e)–8(h), 8(i)–8(l), we depict our calculated Fe d_{xy}, d_{yz+xz}, d_{z^2}, $d_{x^2-y^2}$ orbital-projected DOS for ambient, 15 GPa, and 25 GPa pressure, respectively. It is quite evident from Figs. 8(c), 8(g), and 8(k) that Fe-d_{z^2} orbital derived partial DOS are modified remarkably with the pressure as the Fermi level shifts away

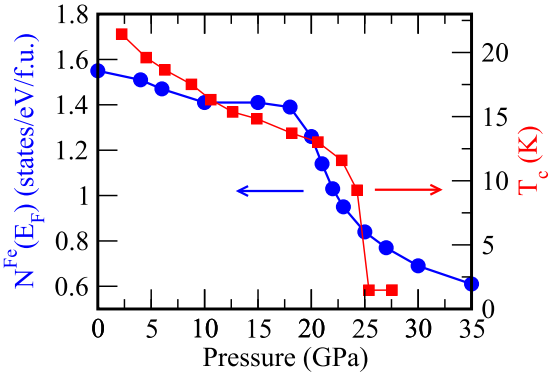

FIG. 7. Fe-*d* orbital-projected density of states at the Fermi level (blue circle) and experimentally measured superconducting T_c [48] (red square) as a function of pressure.

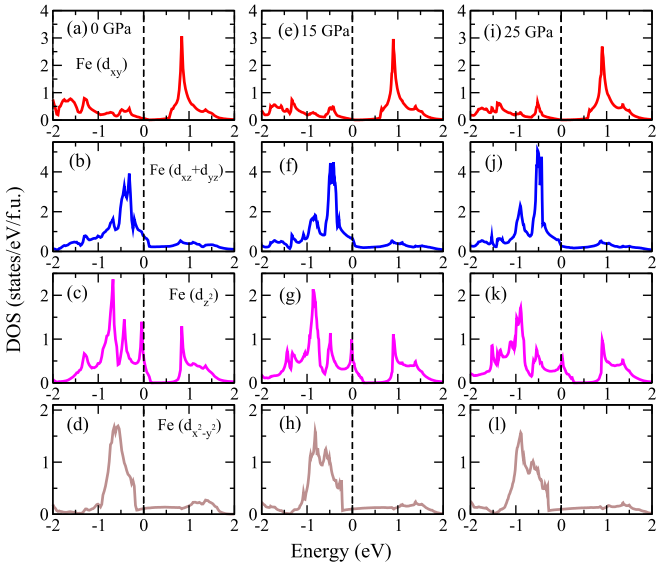

FIG. 8. Calculated orbital-projected density of states of tetragonal ThFeAsN at (a)–(d) ambient, (e)–(h) 15 GPa, and (i)–(l) 25 GPa pressure. d_{xy}, d_{yz+xz}, d_{z^2}, and $d_{x^2-y^2}$ orbitals are indicated by red, blue, magenta, and brown colors, respectively.

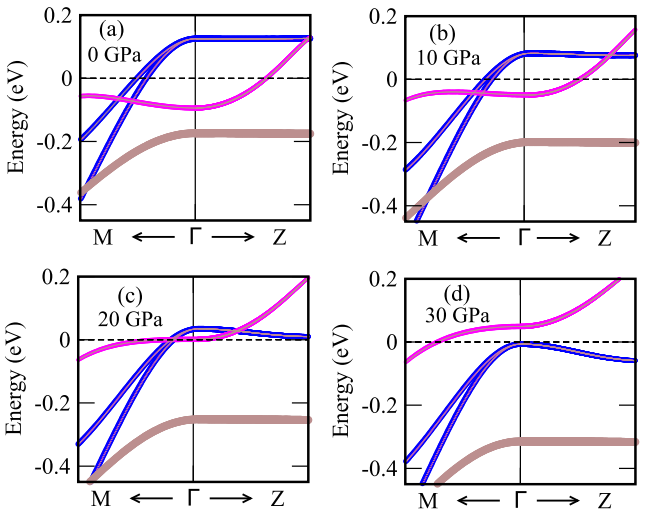

FIG. 10. Calculated Fe-d orbital-projected low energy band structure of ThFeAsN near the Γ point for (a) ambient, (b) 10 GPa, (c) 20 GPa, and (d) 30 GPa pressure. d_{yz+xz}, d_{z^2}, $d_{x^2-y^2}$ orbitals are indicated by blue, magenta, and brown colors, respectively. Here the line thickness denotes the weight of the Fe-d orbitals.

from a van Hove singularity as we go towards higher pressure. On the other hand, we observe the exactly opposite scenario for the degenerate d_{yz+xz} orbital projected DOS. This certainly indicates that orbital characters around the Fermi level at higher pressure and ambient pressure are different from each other.

Next, we see the modifications in the electronic band structure with external pressure. In Fig. 9, we present our calculated low energy (−1 eV to 1 eV) electronic band structures for tetragonal ThFeAsN at different pressures. A number of noticeable modifications are found in the band structures at various hydrostatic pressures. We can clearly see from Fig. 9 that electronic bands around the Γ point are significantly modified as we gradually increase the pressure. On the other hand, hydrostatic pressure hardly modifies the electronic bands near the (M/X) point. In Fig. 10 (Fig. 11), we present the orbital-projected band structure of ThFeAsN around the Γ point (M point) for various hydrostatic pressures. Various Fe-d orbital characters are depicted by different colors (d_{yz+xz}, d_{z^2}, $d_{x^2-y^2}$ orbitals are indicated by blue, magenta, and brown colors, respectively). In Fig. 12, we depict the variation of different band energies around the Γ point with pressure. The band with d_{z^2} orbital character goes above the Fermi level as we move from ambient to higher pressure. This is recognized as Lifshitz transition occurring at around 25 GPa pressure. Degenerate bands with d_{yz+xz} orbital characters around the Γ point also move downwards and touch the Fermi level at

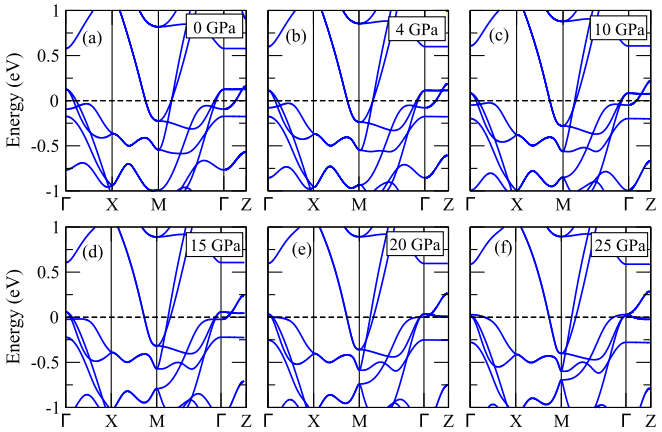

FIG. 9. Calculated band structure of tetragonal ThFeAsN along high symmetry k points at (a) ambient, (b) 4 GPa, (c) 10 GPa, (d) 15 GPa, (e) 20 GPa, and (f) 25 GPa pressure.

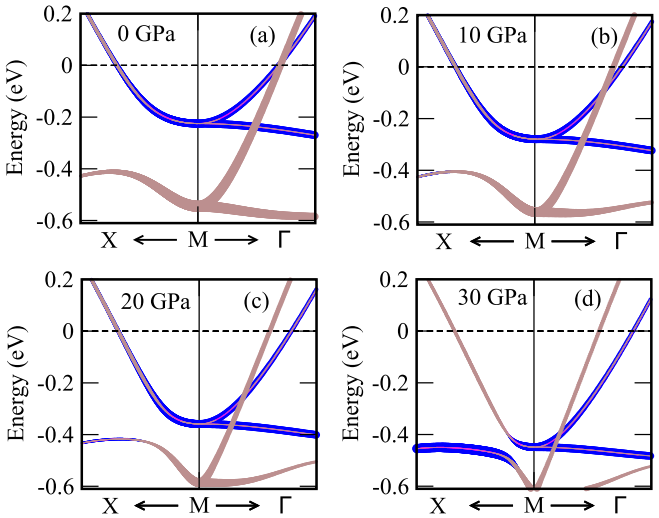

FIG. 11. Calculated Fe-d orbital-projected low energy band structure of ThFeAsN near the M point for (a) ambient, (b) 10 GPa, (c) 20 GPa, and (d) 30 GPa pressure. d_{yz+xz}, d_{z^2}, $d_{x^2-y^2}$ orbitals are indicated by blue, magenta, and brown colors, respectively. Here the line thickness denotes the weight of the Fe-d orbitals.

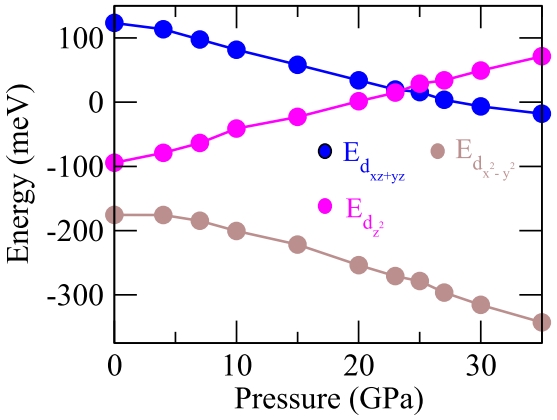

FIG. 12. Variation of different band energies of ThFeAsN around the Γ point with pressure.

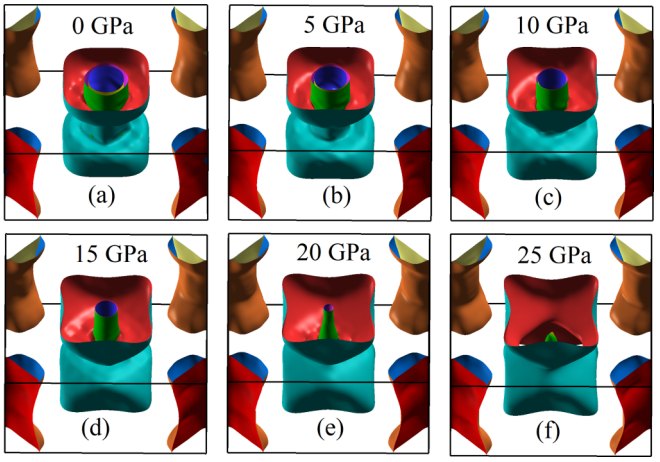

FIG. 13. Calculated Fermi surfaces of tetragonal ThFeAsN at (a) ambient, (b) 5 GPa, (c) 10 GPa, (d) 15 GPa, (e) 20 GPa, and (f) 25 GPa pressure.

30 GPa. On the other hand, the band with predominantly $d_{x^2-y^2}$ character goes down in energy, as we move towards the higher pressure. But the energy dispersion of the $d_{x^2-y^2}$ band is hardly modified by the applied pressure. On the other hand, no such modifications (LT/ETT) in the low energy electronic band dispersion are observed in the vicinity of the M/X point. Therefore, this also can be considered as orbital selective Lifshitz transition. This can change the orbital characters at the Fermi level of ThFeAsN at higher pressure. We should mention here that orbital selective pairing is observed in some Fe-based superconductors such as FeSe [65,66]. Orbital selective pairing means that electrons of predominantly one specific orbital character bind to form the Cooper pairs. As a result, in the FS regions where this specific orbital character dominates, large superconducting gaps appear. This can lead to a highly anisotropic superconducting gaps. Absence of the magnetic order in ThFeAsN makes it a good candidate for orbital selective Cooper pairing (like LiFeAs and FeSe). Due to this orbital selective LT in ThFeAsN, at high pressure, the orbital character near the Fermi level changes from d_{yz+xz} to d_{z^2}. This will change the orbital characters at the Fermi surface of ThFeAsN at higher pressure. We speculate that LT at high pressure will influence the orbital selective pairing which is quite possible in ThFeAsN as evident from the current literature [45]. However, no direct evidence of orbital selective pairing in ThFeAsN has been found from our study. Moreover, the complex nature of intra-inter band pairing in these Fe based SCs makes it even harder to understand the nature of pairing symmetry from the state of the art DFT calculations. Therefore, LTs precisely occur in the holelike bands at the center of the Brillouin zone (Γ point). From Figs. 10 and 11, we can clearly observe that as the pressure increases, the d_{yz+xz} bands near both the Γ and M points become lowered in energy, thus behaving like electron-doped bands. On the other hand, the d_{z^2} band moves upwards with pressure, behaving like being hole doped. This phenomenon can be regarded as orbital selective self-doping. We see in the structural parameters as a function of pressure, in-plane As-As distance varies very little in comparison with the out-of-plane As-As distance [see Fig. 3(c)]. Therefore, orbitals that extend in the xy plane ($d_{x^2-y^2}$) remain almost the same (dispersion) as we increase the pressure. On the other hand, orbitals that extend along the z axis (d_{yz+xz}, d_{z^2},) are modified largely by the external pressure. More precisely, if we see the d_{z^2} band around the Γ point, the nature of band dispersion changes with the pressure. More precisely, the electronlike d_{z^2} band becomes a holelike band at higher pressure. No such electronic topological transitions occur in the bands near the M/X point.

Significant modification in the bands near the Γ point with pressure also indicate that FS topology of ThFeAsN also changes with the external pressure. We show our calculated FSs of the ThFeAsN system at different hydrostatic pressures in Fig. 13. At ambient pressure (0 GPa), there are three holelike FSs at the Γ point and two electronlike FSs at the M point. All the FSs at different pressures are also shown separately in Fig. 14 for better insights. It is quite evident from Fig. 14 that electronlike FSs at the M point are hardly affected by the external pressure. On the contrary, external pressure influences

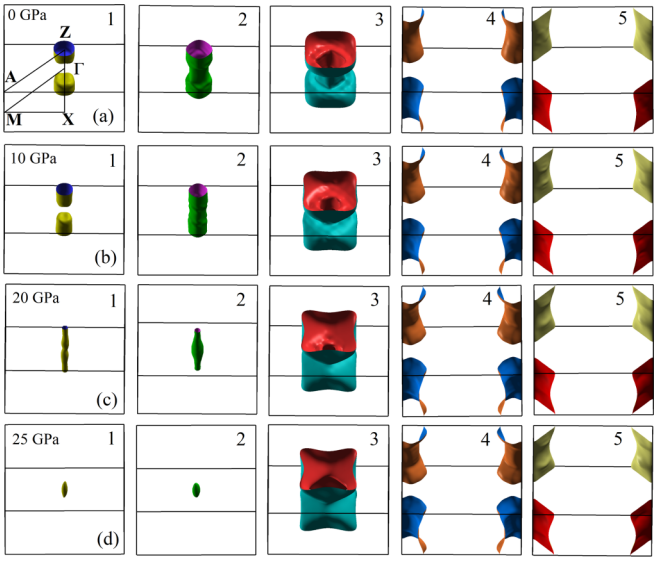

FIG. 14. Evolution of all the electron- and holelike Fermi surfaces at (a) ambient, (b) 10 GPa, (c) 20 GPa, and (d) 25 GPa pressure.

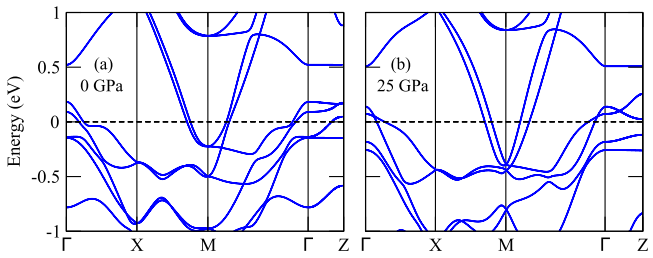

FIG. 15. Calculated band structure of tetragonal ThFeAsN with spin-orbit coupling at (a) ambient pressure and (b) 25 GPa of hydrostatic pressure.

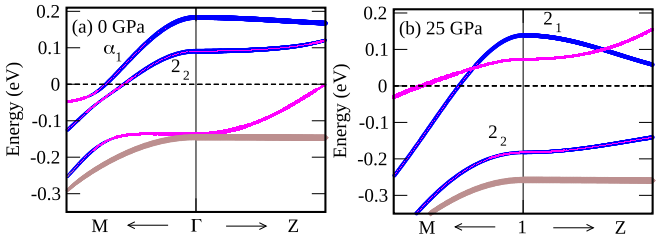

FIG. 16. Calculated Fe-d orbital-projected low energy band structure of ThFeAsN at the Γ point with spin-orbit coupling for (a) ambient and (b) 25 GPa pressure. d_{yz+xz} (α_1, α_2), d_{z^2} (β), $d_{x^2-y^2}$ (γ) orbitals are indicated by blue, magenta, and brown colors, respectively.

the holelike FSs around the Γ point remarkably. Holelike FSs labeled as 1, 2, and 3 completely changed topologically at higher pressure. This evolution of FSs with hydrostatic pressure directly affects the nesting of FS, which is believed to play a key role in the superconductivity of Fe-based SCs. It is also well documented that two-dimensional (2D) FS favors superconductivity in Fe-based SCs (nesting is stronger in 2D FSs as compared to the 3D FSs) [15,67]. But at higher pressure, we find more 3D-like FSs (especially holelike FSs around the Γ point) in contrast to that at the lower pressure. See Appendix B for FSs calculated using experimental structural parameters where the transformation from 2D-like FSs (ambient pressure) to more 3D-like FSs (25 GPa pressure) is very clear. Therefore, we can conclude that pressure induced LT or ETT affects the low energy electronic structures significantly which control the superconducting properties in the ThFeAsN system. Experimentally it has been shown that superconducting transition temperature (T_c) decreases with the increasing pressure. T_c drops sharply to 0 K at around 25 GPa of pressure on the verge of LT. In general, LTs in Fe-based superconductors are largely found to help in growing superconductivity [33,39,68]. For example, in electron doped $BaFe_2As_2$, LTs occur in the holelike bands as the band with d_{xy} orbital character goes below the Fermi level (one of the FS disappears from the Γ point) at the same doping concentration where T_c reaches its maximum value [39]. However, in ThFeAsN superconducting T_c vanishes approximately at the same pressure where LT occurs. Therefore, it is worthy to mention here that the appearance of the band at the Fermi level with d_{z^2} orbital character around the Γ point at higher pressure is a quite unique feature of ThFeAsN superconductor. This makes the ThFeAsN system a unique one, breaking the universal trend of superconductivity and LT/ETT in Fe-based SC.

C. Effect of spin-orbit coupling in electronic structure

In this section, we show the influence of spin-orbit coupling (SOC) on the low energy electronic band structure of ThFeAsN at higher pressure. The structural parameters are hardly affected by SOC. In Fig. 15, we depict our calculated band structures in the presence of SOC for ambient as well as 25 GPa of hydrostatic pressure. Orbital projected (Fe-d orbitals) band structures with SOC at ambient and 25 GPa pressures are presented in Figs. 16(a) and Fig. 16(b), respectively. It is very clear from Fig. 15 and Fig. 16 that with the introduction of SOC, low energy band structures around the Γ point are modified remarkably as the degenerate d_{yz+xz} band near the Fermi level splits into two bands (α_1, α_2) with the same d_{yz+xz} orbital character for both cases (ambient and 25 GPa pressure). LT also occurs in the presence of SOC with pressure as the band (β) with d_{z^2} orbital character around the Γ point moves upward and crosses the Fermi level. The splitting of the d_{yz+xz} band (α_1, α_2) around the Γ point is very large at higher pressure (25 GPa) as compared to that at the ambient pressure. From Fig. 16, we can clearly see that SOC at higher pressure modifies the energy ordering of the orbitals near the Γ point. SOC at higher pressure splits the d_{yz+xz} band around the Γ point such that α_2 goes below the Fermi level whereas in the absence of SOC, the degenerate d_{yz+xz} band (no splitting) goes below the Fermi level (see Fig. 10). Since SOC modifies the energy ordering (or in other words orbital ordering) near the Fermi level at higher pressure, it can affect the superconducting properties [65,66] which probably depend on the orbital character of the FSs. This indicates that SOC may play a crucial role in superconductivity of the ThFeAsN system.

IV. CONCLUSIONS

In this section, we summarize our theoretical results. We have studied pressure dependent structural parameters and electronic structures of the ThFeAsN superconductor. Structural parameters as well as elastic constants show no anomalous behavior with hydrostatic pressure which is consistent with the experimental observation of the absence of structural transition with pressure in the ThFeAsN system. We depict the electronic structures of ThFeAsN at different external pressures. Density of states, band structure, and FS as a function of hydrostatic pressure has been thoroughly investigated. Density of states at the Fermi level, coming from Fe-d orbitals, and superconducting T_c both vary similarly with pressure. We find a pressure induced orbital selective LT in the ThFeAsN compound. This electronic topological transition or Lifshitz transition is quite different by nature from the Lifshitz transitions observed in the other families of Fe-based superconductor (with doping and pressure). FSs of ThFeAsN at the Γ point (holelike) are modified immensely by the application of external pressure. We thus speculate that pressure dependent modification of FS topology, which is a manifestation of LT observed in the electronic band structure

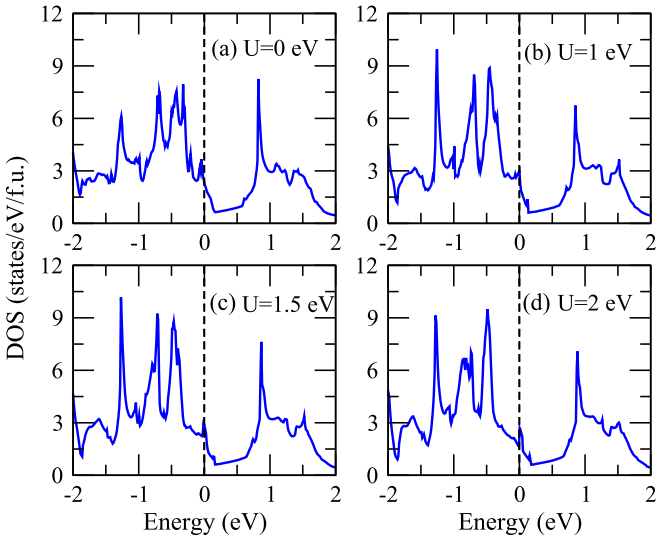

FIG. 17. Calculated DOS of ThFeAsN at ambient pressure within the GGA+U formalism with Hubbard $U = 0$ eV (a), $U =$ 1 eV (b), 1.5 eV (c), and 2 eV (d) on Fe-3d orbitals.

at higher pressure, is mainly responsible for the reduction of superconducting T_c in the ThFeAsN superconductor. In the presence of SOC, LT still occurs at higher pressure. However, a change in the energy ordering of the orbitals is observed at higher pressure with the introduction of SOC.

ACKNOWLEDGMENTS

The authors acknowledge the support from the Ministry of Science and Technology and Far Eastern Y. Z. Hsu science and Technology Memorial Foundation in Taiwan. The authors are also grateful to the National Center for High-performance Computing in Taiwan for computing time.

APPENDIX A: EFFECT OF ONSITE COULOMB REPULSION

In this Appendix, we study the effect of onsite Coulomb repulsion on the electronic structure of ThFeAsN in ambient pressure. We investigate the impact of electronic correlation modeled by the GGA+U scheme [55] with Hubbard U on Fe-3d orbitals. We choose three effective U values and calculate the DOS for each case, and the calculated DOS spectra are presented in Fig. 17. We can see that the DOS of ThFeAsN

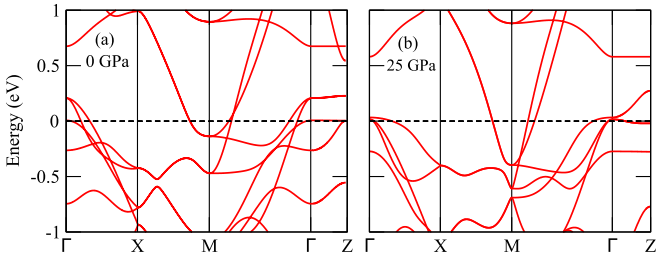

FIG. 18. Calculated band structures of ThFeAsN employing experimental structural parameters (lattice parameters as well as z_{As}) at (a) ambient pressure and (b) 25 GPa of hydrostatic pressure.

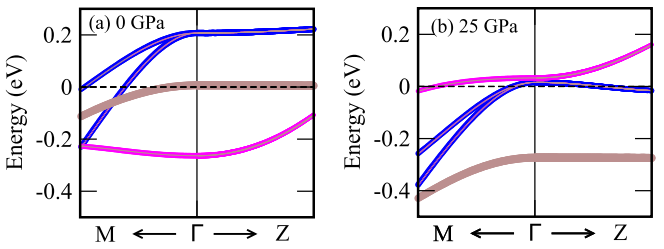

FIG. 19. Calculated Fe-d orbital-projected band structures of ThFeAsN around the Γ point, using experimental structural parameters (lattice parameters as well as z_{As}) at (a) ambient pressure and (b) 25 GPa of hydrostatic pressure.

near the Fermi level is not very affected by the application of Hubbard U on Fe-3d orbitals. The change in the total DOS at the Fermi level is 6% for maximum $U = 2$ eV. In contrast, we observe a 54% decrease in the DOS at the Fermi level with the application of 35 GPa of hydrostatic pressure.

APPENDIX B: ELECTRONIC STRUCTURES CALCULATED USING EXPERIMENTAL STRUCTURAL PARAMETERS

In this Appendix, we present band structures and FSs of ThFeAsN at ambient pressure as well as at 25 GPa of hydrostatic pressure calculated using experimental lattice parameters and experimental z_{As}. Experimental lattice parameters and z_{As} are taken from Ref. [48]. Using these experimental structural parameters, we calculate the band structures of ThFeAsN at 25 GPa pressure as well as at ambient pressure as depicted in Fig. 18. In Fig. 19, we exhibit the orbital-projected band structures around the Γ point for the same. We can clearly see that the band with d_{z^2} orbital character moves upward and goes above the Fermi level at 25 GPa of external pressure. On the other hand, the band with d_{yz+xz} orbital character moves downward as we go to a higher pressure of 25 GPa and touches the Fermi level. Similar evolution of electronic bands with the same orbital characters with external pressure is observed in the case of our calculated band structures using optimized structural parameters. However, the $d_{x^2-y^2}$ band changes remarkably at 25 GPa of pressure from the ambient condition when we use the experimental structural parameters (see Fig. 19). This is the only major difference that we observed in the band structure calculated using experimental structural parameters as compared to that of the optimized one. In Fig. 20, we depict the FSs

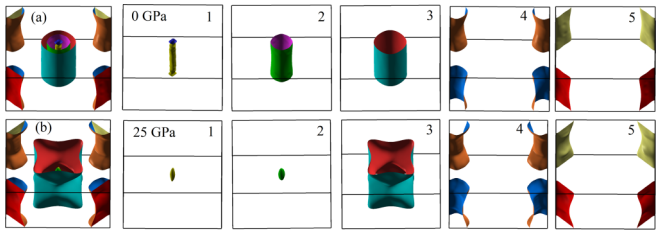

FIG. 20. Evolution of Fermi surfaces of ThFeAsN, calculated using experimental structural parameters (lattice parameters as well as z_{As}) at (a) ambient pressure and (b) 25 GPa of hydrostatic pressure.

of ThFeAsN at ambient pressure and 25 GPa of hydrostatic pressure, calculated using experimental structural parameters. Experimental data produce more two-dimensional holelike FSs around the Γ point than that produced by the optimized structural parameters. However, at higher pressure (25 GPa), FSs calculated using experimental structural parameters become more three dimensional and resemble that of the same calculated using optimized structural parameters. This is more so because of the resemblance of the calculated and experimentally measured structural parameters at higher pressure.

[1] G. R. Stewart, Rev. Mod. Phys. **83**, 1589 (2011).
[2] M. Bendele, A. Ichsanow, Y. Pashkevich, L. Keller, T. Strässle, A. Gusev, E. Pomjakushina, K. Conder, R. Khasanov, and H. Keller, Phys. Rev. B **85**, 064517 (2012).
[3] E. Wiesenmayer, H. Luetkens, G. Pascua, R. Khasanov, A. Amato, H. Potts, B. Banusch, H.-H. Klauss, and D. Johrendt, Phys. Rev. Lett. **107**, 237001 (2011).
[4] P. Materne, S. Kamusella, R. Sarkar, T. Goltz, J. Spehling, H. Maeter, L. Harnagea, S. Wurmehl, B. Büchner, H. Luetkens, C. Timm, and H.-H. Klauss, Phys. Rev. B **92**, 134511 (2015).
[5] L. Wang, F. Hardy, A. E. Böhmer, T. Wolf, P. Schweiss, and C. Meingast, Phys. Rev. B **93**, 014514 (2016).
[6] J. Dong, H. J. Zhang, G. Xu, Z. Li, G. Li, W. Z. Hu, D. Wu, G. F. Chen, X. Dai, J. L. Luo, Z. Fang, and N. L. Wang, Europhys. Lett. **83**, 27006 (2008).
[7] V. Cvetkovic and Z. Tesanovic, Europhys. Lett. **85**, 37002 (2009).
[8] V. Cvetkovic and Z. Tesanovic, Phys. Rev. B **80**, 024512 (2009).
[9] R. M. Fernandes, A. V. Chubukov, and J. Schmalian, Nat. Phys. **10**, 97 (2014).
[10] R. M. Fernandes, L. H. VanBebber, S. Bhattacharya, P. Chandra, V. Keppens, D. Mandrus, M. A. McGuire, B. C. Sales, A. S. Sefat, and J. Schmalian, Phys. Rev. Lett. **105**, 157003 (2010).
[11] C.-C. Lee, W.-G. Yin, and W. Ku, Phys. Rev. Lett. **103**, 267001 (2009).
[12] F. Kruger, S. Kumar, J. Zaanen, and J. van den Brink, Phys. Rev. B **79**, 054504 (2009).
[13] W. Lv, J. Wu, and P. Phillips, Phys. Rev. B **80**, 224506 (2009).
[14] R. S. Dhaka, C. Liu, R. M. Fernandes, R. Jiang, C. P. Strehlow, T. Kondo, A. Thaler, J. Schmalian, S. L. Bud'ko, P. C. Canfield, and A. Kaminski, Phys. Rev. Lett. **107**, 267002 (2011).
[15] S. Sen and H. Ghosh, Phys. Lett. A **379**, 843 (2015).
[16] D. J. Singh and M.-H. Du, Phys. Rev. Lett. **100**, 237003 (2008).
[17] R. S. Dhaka, S. E. Hahn, E. Razzoli, R. Jiang, M. Shi, B. N. Harmon, A. Thaler, S. L. Bud'ko, P. C. Canfield, and A. Kaminski, Phys. Rev. Lett. **110**, 067002 (2013).
[18] S Sen, H. Ghosh, A. K. Sinha, and A. Bharathi, Supercond. Sci. Technol. **27**, 122003 (2014).
[19] K. Quader and M. Widom, Phys. Rev. B **90**, 144512 (2014).
[20] X. H. Chen, P. C. Dai, D. L. Feng, T. Xiang, and F. C. Zhang, Nat. Sci. Rev. **1**, 371 (2014).
[21] A. S. Sefat, Rep. Prog. Phys. **74**, 124502 (2011).
[22] A. S. Sefat and D. J. Singh, Mater. Research Soc. Bull. **36**, 614 (2011).
[23] M. S. Torikachvili, S. L. Bud'ko, N. Ni, P. C. Canfield, and S. T. Hannahs, Phys. Rev. B **80**, 014521 (2009).
[24] A. Mani, S. Ghost, S. Paulraj, A. Bharathi, and C. S. Sundar, Europhys. Lett. **87**, 17004 (2009).
[25] S. R. Saha, N. P. Butch, T. Drye, J. Magill, S. Ziemak, K. Kirshenbaum, P. Y. Zavalij, J. W. Lynn, and J. Paglione, Phys. Rev. B **85**, 024525 (2012).
[26] T. M. McQueen, I. A. Troyan, T. Palasyuk, M. I. Eremets, R. J. Cava, S. Naghavi, F. Casper, V. Ksenofontov, G. Wortmann, and C. Felser, Nat. Mater. **8**, 630 (2009).
[27] D. Kasinathan, A. Ormeci, K. Koch, U. Burkhardt, W. Schnelle, A. L.-Jasper, and H. Rosner, New J. Phys. **11**, 025023 (2009).
[28] Y. Mizuguchi, Y. Hara, K. Deguchi, S. Tsuda, T. Yamaguchi, K. Takeda, H. Kotegawa, H. Tou, and Y. Takano, Supercond. Sci. Technol. **23**, 054013 (2010).
[29] J. Wu, P. Phillips, and A. H. Castro Neto, Phys. Rev. Lett. **101**, 126401 (2008).
[30] R. P. Day, G. Levy, M. Michiardi, B. Zwartsenberg, M. Zonno, F. Ji, E. Razzoli, F. Boschini, S. Chi, R. Liang, P. K. Das, I. Vobornik, J. Fujii, W. N. Hardy, D. A. Bonn, I. S. Elfimov, and A. Damascelli, Phys. Rev. Lett. **121**, 076401 (2018).
[31] P. D. Johnson, H.-B. Yang, J. D. Rameau, G. D. Gu, Z.-H. Pan, T. Valla, M. Weinert, and A. V. Fedorov, Phys. Rev. Lett. **114**, 167001 (2015).
[32] I. M. Lifshitz, Sov. Phys. JETP **11**, 1130 (1960).
[33] S. N. Khan and D. D. Johnson, Phys. Rev. Lett. **112**, 156401 (2014).
[34] N. Xu, P. Richard, X. Shi, A. van Roekeghem, T. Qian, E. Razzoli, E. Rienks, G.-F. Chen, E. Ieki, K. Nakayama, T. Sato, T. Takahashi, M. Shi, and H. Ding, Phys. Rev. B **88**, 220508(R) (2013).
[35] A. Ghosh, H. Ghosh, and S. Sen, Intermetallics **107**, 126 (2019).
[36] C. Liu, T. Kondo, R. M. Fernandes, A. D. Palczewski, E. D. Mun, N. Ni, A. N. Thaler, A. Bostwick, E. Rotenberg, J. Schmalian, S. L. Bud'ko, P. C. Canfield, and A. Kaminski, Nat. Phys. **6**, 419 (2010).
[37] H. Ghosh and S. Sen, J. Alloys Compd. **677**, 245 (2016).
[38] K. Nakayama, T. Sato, P. Richard, Y.-M. Xu, T. Kawahara, K. Umezawa, T. Qian, M. Neupane, G. F. Chen, H. Ding, and T. Takahashi, Phys. Rev. B **83**, 020501(R) (2011).
[39] H. Ghosh and S. Sen, J. Phys. Chem. Solids **103**, 170 (2017).
[40] Y. Liu and T. A. Lograsso, Phys. Rev. B **90**, 224508 (2014).
[41] A. Varlamov, V. Edorov, and A. Pantsulaya, Adv. Phys. **38**, 469 (1989).
[42] J. Fink, S. Thirupathaiah, R. Ovsyannikov, H. A. Dürr, R. Follath, Y. Huang, S. de Jong, M. S. Golden, Yu-Zhong Zhang, H. O. Jeschke, R. Valentí, C. Felser, S. Dastjani Farahani, M. Rotter, and D. Johrendt, Phys. Rev. B **79**, 155118 (2009).
[43] C. Liu, A. D. Palczewski, R. S. Dhaka, T. Kondo, R. M. Fernandes, E. D. Mun, H. Hodovanets, A. N. Thaler, J. Schmalian, S. L. Bud'ko, P. C. Canfield, and A. Kaminski, Phys. Rev. B **84**, 020509(R) (2011).
[44] C. Wang, Z.-C. Wang, Y.-X. Mei, Y.-K. Li, L. Li, Z.-T. Tang, Y. Liu, P. Zhang, H.-F. Zhai, Z.-A. Xu, and G.-H. Cao, J. Am. Chem. Soc. **138**, 2170 (2016).
[45] T. Shiroka, T. Shang, C. Wang, G.-H. Cao, I. Eremin, H.-R. Ott, and J. Mesot, Nat. Commun. **8**, 156 (2017).
[46] H. Mao, C. Wang, H. E. Maynard-Casely, Q. Huang, Z. Wang, G. Cao, S. Li, and H. Luo, Europhys. Lett. **117**, 57005 (2017).

[47] S. Sen and G.-Y. Guo, arXiv:2005.04579.
[48] H. Wang, J. Guo, Y. Shao, C. Wang, S. Cai, Z. Wang, X. Li, Y. Li, G. Cao, and Q. Wu, Europhys. Lett. **123**, 67004 (2018).
[49] N. Barbero, S. Holenstein, T. Shang, Z. Shermadini, F. Lochner, I. Eremin, C. Wang, G.-H. Cao, R. Khasanov, H.-R. Ott, J. Mesot, and T. Shiroka, Phys. Rev. B **97**, 140506(R) (2018).
[50] G. Kresse and J. Hafner, Phys. Rev. B **47**, 558 (1993).
[51] P. E. Blöchl, Phys. Rev. B **50**, 17953 (1994).
[52] G. Kresse and J. Furthmuller, Comput. Mater. Sci. **6**, 15 (1996).
[53] J. P. Perdew, K. Burke, and M. Ernzerhof, Phys. Rev. Lett. **77**, 3865 (1996).
[54] M. Yi, Y. Zhang, Z.-X. Shen, and D. Lu, npj Q. Mat. **2**, 57 (2017).
[55] S. L. Dudarev, G. A. Botton, S. Y. Savrasov, C. J. Humphreys, and A. P. Sutton, Phys. Rev. B **57**, 1505 (1998).
[56] Y. Le Page and P. Saxe, Phys. Rev. B **65**, 104104 (2002).
[57] L. M. N. Konzen and A. S. Sefat, J. Phys.: Condens. Matter **29**, 083001 (2017).
[58] I. I. Mazin, D. J. Singh, M. D. Johannes, and M. H. Du, Phys. Rev. Lett. **101**, 057003 (2008).
[59] S. Sharma, A. Bharathi, K. Vinod, C. S. Sundar, V. Srihari, S. Sen, H. Ghosh, A. K. Sinha, and S. K. Deb, Acta Cryst. B **71**, 61 (2015).
[60] D. J. Singh, Phys. Rev. B **78**, 094511 (2008).
[61] H. Nakamura and M. Machida, Physica C **494**, 9 (2013).
[62] F. Ricci and G. Profeta, Phys. Rev. B **87**, 184105 (2013).
[63] S. Grimme, J. Antony, S. Ehrlich, and S. Krieg, J. Chem. Phys. **132**, 154104 (2010).
[64] M. Born and K. Huang, *Dynamical Theory of Crystal Lattices* (Oxford University Press, Oxford, 1998).
[65] E. M. Nica, R. Yu, and Q. Si, npj Q. Mat. **2**, 26 (2017).
[66] A. Kreisel, B. M. Andersen, P. O. Sprau, A. Kostin, J. C. Séamus Davis, and P. J. Hirschfeld, Phys. Rev. B **95**, 174504 (2017).
[67] M. Sunagawa, T. Ishiga, K. Tsubota, T. Jabuchi, J. Sonoyama, K. Iba, K. Kudo, M. Nohara, K. Ono, H. Kumigashira, T. Matsushita, M. Arita, K. Shimada, H. Na-matame, M. Taniguchi, T. Wakita, Y. Muraoka, and T. Yokoya, Sci. Rep. **4**, 4381 (2014).
[68] B. Lei, J. H. Cui, Z. J. Xiang, C. Shang, N. Z. Wang, G. J. Ye, X. G. Luo, T. Wu, Z. Sun, and X. H. Chen, Phys. Rev. Lett. **116**, 077002 (2016).